RSC Advances

ROYAL SOCIETY OF CHEMISTRY

www.rsc.org/advances

A novel signal amplification strategy of electrochemical immunosensor for human chorionic gonadotropin based on nanocomposites of multi-walled carbon nanotubes - ionic liquid and nanoporous Pd

Wenjuan Guo, Yiming Liu, Xue Meng, Meishan Pei*, Jinping Wang, Luyan Wang

Shandong Provincial Key Laboratory of Chemical Sensing & Analysis, School of Chemistry and Chemical Engineering, University of Jinan, Jinan 250022, China

*Corresponding author. Tel: +86-18678290022

E-mail: chm_peims@ujn.edu.cn

Abstract

A sensitive label-free immunosensor adopting a novel signal amplification strategy was proposed for electrochemical detection of human chorionic gonadotropin (hCG). Firstly, a novel composite film consisted of multi-walled carbon nanotubes (MWCNTs) and room temperature ionic liquid (RTIL) of 1-butyl-3-methylimidazolium hexafluorophosphate ($BMIMPF_6$), which combined the advantages of MWCNTs and RTIL, was fabricated onto glassy carbon electrode surface. The mechanism of the synergy of MWCNTs and RTIL has been discussed. Secondly, nanoporous Pd (NP-Pd) prepared by simple dealloying method was modified on the first film. The structure of NP-Pd has been confirmed by EDS, XRD, SEM, TEM and BET analysis. Due to the large specific surface area and excellent electrical conductivity of NP-Pd, $K_3[Fe(CN)_6]$ as electron transfer mediator was promoted and the amount of hCG antibody was enhanced significantly. Results showed that MWCNTs-$BMIMPF_6$/NP-Pd composites were successfully designed to be a sensitive immunosensor platform for hCG determination. Under the optimum conditions, the immunosensor exhibited high senstitivity and a wide linear range for hCG from 0.05 to 50 ng mL^{-1} with a detection limit of 3.2 pg mL^{-1}. The prepared immunosensor showed high sensitivity, reproducibility and stability. And this immunosensor preparation strategy was a promising platform for clinical application.

Keywords: Electrochemical immunosensor, Multi-walled carbon nanotubes, Ionic liquid, Nanoporous Pd, hCG

Introduction

Human chorionic gonadotropin (hCG) exists in blood and urine of pregnant women. It can be used as a tumor marker especially in gestational trophoblastic disease. It is very important for early diagnose of hCG produced by placenta in clinical use to prevent the spread of pregnancy complications [1-3]. Many methods such as fluoroimmunoassay [4, 5], resonance scttering spetral assay [6], spectrometry [7], and electrochemical immunosensors [8-10] have been developed to detect hCG. Among these techniques mentioned above, electrochemical sensors [11, 12] continue to be popular in the last decade due to their high sensitivity, inherent simplicity, low cost, and rapid detection. The modifying technology of the electrode is the crucial step, which affects the signal intensity of the electrochemical detection and the immobilization of biological molecule. Thus, it is necessary to develop a simple immobilization method to form the efficient matrices to improve the performance of electrochemical immunosensors.

Among various immobilization methods, the traditional method was to form covalent coupling, which provided the stable and strong bind between the desired biomolecule and the electrode substrate. In this method, some molecules, such as 1-ethyl-3-(3-dimethylaminopropyl)-carbodiimide (EDC) and N-hydroxysuccinimide (NHS), were usually applied to make the functional groups of the substrate or the desired biomolecule active [13-15]. The complicated chemical reaction had some drawbacks [16], such as cumbersome and time-consuming in practice. Therefore, looking for a new fabrication technology has become a hot research topic.

With the development of the nanoporous metallic materials, such as Au, Pt and Pd-based metals, it has been proved that the nanoporous metals are the ideal materials which can form immobilization matrices easily and amplify signal [17-19]. Research works in the field of nanotechnology [20, 21] has proved that nanoporous nanomaterials are the excellent materials to be used in the electrochemical sensors [22-25]. Nanoporous metals [26, 27] have received considerable attention due to their high surface area and three-dimensional (3D) interconnected network structure. In this work, nanoporous Pd (NP-Pd), prepared by simple dealloying method, was applied not only to provide the higher surface area for the conjugation of antibody but also to facilitate the electron transfer. The surface of NP-Pd prepared in concentrated alkaline solution (without any surfactants) was extremely clean, which was beneficial for its application in the further experiments without any purification. Therefore, NP-Pd provides the unprecedented promise in electrochemical assay.

Till now, different signal amplification strategies [28, 29] have been developed to improve the performance of the electrochemical immunosensors. Carbon nanotubes (CNTs) [30-32] as typical nanomaterial have attracted wide attention in electroanalysis. CNTs play an important role in improving sensor performance due to their unique structure and extraordinary physical properties, such as large ratio of surface area to mass ultralight weight, high electrical conductivity, and remarkable mechanical strength. Many applications of CNTs in electrochemical sensing and bioelectrochemistry [33, 34] have been reported. Nevertheless, the development of CNT-based sensing devices is encumbered by the low solubility of CNTs in most

solvents. Therefore, there is a pressing need to find pathways that can overcome above obstacle. Fortunately, it is found that CNTs could be considerably untangled into much finer bundles in room temperature ionic liquids (RTIL). RTIL possess unique physicochemical characters, such as high ionic conductivity, wide electrochemical windows, good chemical and thermal stability, and negligible vapour pressure [35-37], which make them to be suitably used as the surpporting electrolyte or the modifier in electroanalysis. More interestingly, the capability of RTIL combining with carbon materials to form novel conductive compositemakes them very attractive for the preparation of various electrodes with good conductivity [38].

In this work, a novel label-free immunosensors of hCG was fabricated by utilizing multi-walled carbon nanotubes (MWCNTs)-1-butyl-3-methylimidazolium hexafluorophosphate ($BMIMPF_6$) (MWCNTs-$BMIMPF_6$) and NP-Pd as the matrix. MWCNTs-$BMIMPF_6$ composites were used as an effective load matrix for NP-Pd and the electrochemical signal was enhanced greatly by the synergistic amplification effect of the two kinds of excellent nanomaterials, NP-Pd and MWCNTs. The modified electrode exhibited excellent sensitivity, selectivity and stability for the determination of hCG. Most importantly, MWCNTs-$BMIMPF_6$/NP-Pd has been used in a label-free immunosensor for the selective detection of hCG for the first time. Under the optimum conditions, the as-prepared immunosensor showed a wide linear range with low detection limit. The practical application of the as-prepared immunosensor for the determination of hCG in human serum was also fulfilled. The as-prepared immunosensor may provide potential applications for the ultrasensitive

detection of different biomolecule.

Experimental

Reagents and materials

MWCNTs were purchased from Beijing Dekedaojin technology Co., Ltd. (China). $BMIMPF_6$ were purchased from from Sigma-Aldrich (St. Louis, MO, USA). Ag, hCG antibody (Ab), carcinoembryonic antigen (CEA) and alfa fetoprotein (AFP) were purchased from Shanghai Lingcao Biotechnology Co., Ltd. (China). N,N-dimethylformamide (DMF), bovine serum albumin (BSA), Urea, L-tyrosine sulfate, methionine, DL-typtophan, ascorbic acid (Vc), L-glutamic acid, folic acid and sucrose were purchased from Sinopharm Chemical Reagent Co., Ltd. (China). Other chemicals and solvents were of guaranteed analytical grade. Ultrapure water was used in all experiments.

Apparatus

Electrochemical measurements were performed on a CHI 760E electrochemical working station (Shanghai Chenhua Instrument, China. Electrochemical impedance measurement (EIS) was performed on Zennium electrochemical workstation (Zahner, Germany). All electrochemical measurements were done in an unstirred electrochemical cell at room temperature. X-ray diffraction (XRD) analysis was carried out on a Bruker D8 advanced X-ray diffractometer. The NP-Pd sample was tablet for the images of scanning electron microscope (SEM) on QUANTA PEG 250 with energy dispersive X-ray spectrometer (EDS), and the sample was dispersed in solvent for transmission electron microscopy (TEM) on JEM-2100. The

Barunauer-Emmett-Teller (BET) analysis was using nitrogen adsorption instrument (America, Quantachrome).

Synthesis of NP-Pd

The NP-Pd was prepared according to literature [39]. PdAl alloy foils were made by refining pure (>99.9%) Pd and Al under the protection of argon atmosphere in a furnace, followed by melt-spinning. Then the NP-Pd was gained by dipping PdAl alloy foils in 1 M NaOH solutions at room temperature for 24 h. During the dealloying process, Pd atoms left behind would self-organize into an interconnected network of pores and ligaments in terms of effective predetermination of the metallic composition and the foils became brittle. After dealloying, the foils were crushed to uniformed grain by a mortar prior to characterization. 5 mg of NP-Pd was dispersed in 1 mL of 1 wt% chitosan (CS) under sonication to obtain a black suspension.

Preparation of MWCNTs-BMIMPF$_6$

4 mg of MWCNTs was dispersed in 1.5 mL CS. 0.05 g of BMIMPF$_6$ was added into 0.5 mL DMF. MWCNTs-BMIMPF$_6$ composite was prepared by mixing the above mixture under sonication to obtain a homogeneous dispersion.

Fabrication of the immunosensor

Scheme 1 displays the stepwise procedure of the immunosensor. The GCE was polished to a mirror finish with 0.3 and 0.05 μm alumina slurry, and then thoroughly washed ultrasonically in ethanol and ultrapure water in turn. 5 μL mixture of MWCNTs- BMIMPF$_6$ was placed on the surface of GCE. Next, 5 μL of NP-Pd (5 mg mL^{-1}) was dropped onto the electrode surface to immobilize Ab. The electrode was

thoroughly rinsed with PBS to remove unbounded particles. Subsequently, 10 μL of prepared excessive Ab solution (10 μg mL^{-1}) was added onto the modified working electrode and incubated for 12 h. The modified working electrode was then washed with PBS to remove nonspecific physically adsorption and immersed in 1% BSA solution for 1 h at 4 ℃ to block nonspecific binding sites between Ab and electrode surface. Finally, the electrode was incubated in a varying concentration of hCG solution for 2 h. Each step was washed by PBS thoroughly for several times. The electrode was stored in the refrigerator prior to use. Cyclic voltammetrys (CVs) was recorded in PBS. After the background current was stabilized, the change in the current response (I) before and after antigen–antibody reaction was recorded.

(Scheme 1)

Detection of hCG

Electrochemical measurements were performed with a conventional three-electrode system composed of a glassy carbon working electrode (GCE), a platinum wire counter electrode, and Ag/AgCl reference electrode. Cyclic voltammetry (CV) was carried out at a scan rate of 100 mV s^{-1} in PBS. After the background current was stabilized, the change in the current response (I) before and after antigen–antibody reaction was recorded.

Results and discussion

Characterization of MWCNTs-$BMIMPF_6$

SEM was used to examine the morphologies of the MWCNTs and MWCNTs-$BMIMPF_6$. As shown in Fig. 1(a), MWCNTs were highly entangled with

one another, which could be attributed to π-π stacking interaction between MWCNTs. In the bundle, MWCNTs adhere tightly according to the previous studies [40, 41]. Thus, MWCNTs are difficult to be dispersed by ordinary solvents. While in Fig. 1(b), in the case of MWCNTs-$BMIMPF_6$, the surface morphology was distinctly different from the MWCNTs. The heavily entangled MWCNTs bundles were found to be untangle within $BMIMPF_6$. This might be ascribed to strong π-π stacking interactions [41, 42] and weak "cation-π" interaction [41, 43, 44] between MWCNTs and RTIL. [$BMIM^+$] (Fig. 2) consist of imidazole ring and alkyl chain. Imidazole ring possesses π-conjugated structure, and positive charge is mainly localized in imidazole ring. π-electron and cations in $BMIMPF_6$ could interact with π-electron in MWCNTs. Additionally, the dielectric constants of RTIL are normally very large. When MWCNTs and $BMIMPF_6$ were mixed with CS and DMF by sonicating, MWCNTs were detached from the bundles by the shear force. $BMIMPF_6$ could prevent the detached MWCNTs from rebunding by shielding the π-π stacking interaction between MWCNTs. The high surface energy of the detached MWCNTs was effectively appeased since they were enveloped by RTIL via strong π-π stacking interactions and weak "cation-π" interaction between MWCNTs and $BMIMPF_6$. Therefore, it could deduce that $BMIMPF_6$ played an important role in dispersing MWCNTs.

(Fig. 1)

(Fig. 2)

Characterization of the prepared NP-Pd

The composition of NP-Pd sample was monitored by EDS (Fig. 3(a)). Results

proved that the nanoporous material was composed of Pd with few Al atoms. XRD analysis was also used to characterize the dealloyed sample. As shown in Fig. 3(b), it was observed that four diffraction peaks emerged around 40.118◦, 46.658◦, 68.119◦, 82.098◦ (2q), which could be assigned to the diffraction from the (111), (200), (220) and (311) for Pd alloy structure.

Fig. 3(c) showed the SEM image of the dealloyed sample. It was observed that the dealloyed sample was composed of a number of ultrafine nanoporous, and had an open bicontinuous spongy-like morphology. TEM images (Fig. 3(d)(e)) provide more details for the structure. The clear contrast between the bright pores and the dark ligament further confirmed the formation of 3D bicontinuous pore-ligament structure, which is beneficial for the mass and electron transport during electrochemical sensing. It is consistent with the SEM observation.

Pore size and pore size distributions are critical factors for porous materials. Pore size distributions of the sample were confirmed by BET analysis. It could be observed that the pore size of the materials was relatively narrow distributed from Fig. 3(f). The pore size was 5.1 nm.

Based on the above results, Pd alloy with 3D bicontinuous pore-ligament structure was straightforwardly obtained by simple dealloying procedure. Dealloying of alloys is in sharp contrast to the traditional approach of chemical synthesis, where the feeding ratio of metal salts does not guarantee a same nominal composition in the final alloy sample, mainly due to the different reducing rates of individual metal salts [45]. Furthermore, this method can achieve a nearly 100% yield.

(Fig. 3)

Electrochemical characteristics of the modified electrodes

The electrochemical behaviors of bare GCE and modified GCE were studied by taking potassium ferricyanide as electrochemical probe (Fig. 4). A couple of reversible redox peaks of probes could be observed on the bare GCE, indicating a reversible electrochemical process. It is noticeable that the peak current was larger than that of bare GCE after coating with MWCNTs or NP-Pd, suggesting that the introduction of MWCNTs or NP-Pd played an important role in the enhancement of its conductivity and active electrode area. Moreover, it could be clearly seen that the current of NP-Pd/GCE was superior to that of MWCNTs/GCE due to NP-Pd's higher capability of electron transfer. The electrochemical performance of the NP-Pd/MWCNTs/GCE was also superior to that of MWCNTs/GCE and NP-Pd/GCE, which could be ascribed to the synergistic amplification effect of the two kinds of nanomaterials, NP-Pd and MWCNTs. The peak current of MWCNTs-$BMIMPF_6$/GCE showed higher current in comparison with bare GCE and MWCNTs/GCE, which indicated that the presence of $BMIMPF_6$ could increase the peak current. Additionally, after modification of the MWCNTs-$BMIMPF_6$/GCE with NP-Pd, the peak current further increased distinctly, suggesting that the NP-Pd/MWCNTs-$BMIMPF_6$ film on GCE could further increase electron transfer rate. NP-Pd/MWCNTs-$BMIMPF_6$/GCE showed increase in current in contrast with NP-Pd/MWCNTs/GCE, which implied that the rate of electron transfer was faster, due to the synergic effect of MWCNTs and $BMIMPF_6$. Based on the observation, MWCNTs-$BMIMPF_6$ composite film was fit

for the effective load matrix for NP-Pd. Therefore, it demonstrated that the combination of $BMIMPF_6$ and MWCNTs could bring an advanced and sensitive electrode substrate and the introduction of NP-Pd was believed to offer unprecedented benefits in catalysis design, which might be a new idea for the construction of novel and powerful electrochemical sensors.

(Fig. 4)

In order to further confirm above speculation, the surface coverage (Γ^*) of the six kinds of electrodes were evaluated from the equation [46]:

$$Q=nFA\Gamma^*$$

Where Q is quantity of electric charge, n is the transferring electron number and A is electroactive surface area. The average electroactive surface areas could be calculated based on the Randles–Sevcik equation [47, 48]:

$$I_p=2.65\times10^5\, n^{3/2}\, AD^{1/2}\, \nu^{1/2}\, c$$

where I_p is the peak current, D is the diffusion coefficient of the redox probe, ν is the scan rate and C is the bulk concentration of the oxidized form. For $K_3[Fe(CN)_6]$, n=1, $D=7.0\times10^{-6}$ cm^2 s^{-1}. The calculated results were revealed in Table 1. The surface coverage of the NP-Pd depositing on the MWCNTs-$BMIMPF_6$/GCE was larger than that of other modified electrode, which further proved that the modified electrode combined the superior characteristics of MWCNTs and RTIL. This was related to their interaction. MWCNTs bundles could be considerably untangled within $BMIMPF_6$, resulting in greatly increasing the effective area of the electrode to load more NP-Pd. In addition, it migh be because MWCNTs and $BMIMPF_6$ could interact

with NP-Pd through hydrophobic interaction, so as to facilitate the deposition of NP-Pd [35].

(Table 1)

Characterization of the immunosensor fabrication

CVs, an effective and convenient method for probing the feature of the modified electrode, was used to characterize the fabrication of the proposed immunosensor. After treatment with MWCNTs-$BMIMPF_6$, obvious increase in peak current happened (Fig. 5A(b)), indicated that MWCNTs-$BMIMPF_6$ made it easier for the electron transfer. The magnitude of the peak current increased (Fig. 5A(c)) due to the increment of electrode surface area when NP-Pd was coated on the MWCNTs-$BMIMPF_6$ matrix. Nevertheless, after Ab was loaded into channel of NP-Pd through adsorption, an obvious decrease in amperometric response was obtained (Fig. 5A(d)). Because Ab, as biomacromolecules, has weak conductivity, so as to generate the insulating layer and hinder the diffusion of the redox marker toward the electrode surface and hinder electron transfer. After BSA was employed to block the nonspecific binding sites, a successive decrease in the current was observed (Fig. 5A(e)) for the hinder effect of protein on electron transfer. Subsequently, the reaction between Ab/NP-Pd/MWCNTs-$BMIMPF_6$/GCE and hCG has led to further reduction in peak currents (Fig. 5A(f)), which could be attributed to the formation of an immunocomplex blocking layer.

In order to get insight of the fabrication process of the immunosensor, Fig. 5B represented the Nyquist plots of the electrochemical impedance spectroscope (EIS) of

variously modified electrodes. One of the important advantages of EIS over other electrochemical techniques is the small amplitude perturbation from steady state, which makes it possible to treat the response theoretically by linearised or otherwise simplified current-potential characteristics. EIS was performed in a background solution of 5 mM $K_3[Fe(CN)_6]$ containing 0.2 M KCl. In EIS, the electron transfer resistance (R_{et}) could be estimated from the semicircle diameter which was at the high frequencies corresponding to the electron transfer-limited process. It is observed that the bare GCE showed a relatively large resistance. After deposition of NP-Pd/MWCNTs-$BMIMPF_6$ composites, a remarkable decrease in the EIS value was observed (Fig. 6B(a-c)), implying that NP-Pd/MWCNTs-$BMIMPF_6$ composites could promote electron transfer. However, Ab with weak conductivity which could resist electron transfer kinetics of the redox pobe at the interface of electrode was assembled onto NP-Pd/MWCNTs-$BMIMPF_6$/GCE (Fig. 6B(d)), so as to increase the resistance. Similarly, the capture of BSA and hCG resulted in the increase of impedance of the electrode (Fig. 6B(e)(f)). Results showed that BSA and hCG have been successively assembled onto the GCE.

(Fig. 5)

Based on above results, it was confirmed that the fabrication program was feasible and the proposed immunosnesor was successfully fabricated.

Optimization of the immunoassay procedure

The amperometric signal will be affected by the mass ratio of MWCNTs and $BMIMPF_6$, and further influence the electrochemical performance of immunosensor.

As shown in Fig. 6(a), the highest value of electrochemical response was achieved at 2.0 : 25 among different ratio ranging from 1.0 : 25 to 3.0 : 25. The reason might put down to the solvent effect of RTIL. If there was too much $BMIMPF_6$, MWCNTs could be wrapped up by $BMIMPF_6$, so as to counteract the advantage of MWCNTs.

Solution pH has great effects on both the bioactivity of immobilized immunoproteins, but also the electrochemical performance of GCE. In order to optimize the pH, a series of PBS buffer with the pH from 5.8 to 8.0 were prepared. The amperometric signal decreased at strong acidic and alkaline solution. It might be on account of the irreversible behavior of denaturation of proteins involved in the process which was caused by the pH. The optimal response was obtained at pH 7.2 (Fig. 6(b)), which indicated that the weak alkaline environment was more conducive for the antibody to be in operation. Thus, pH 7.2 was chosen as the optimal pH value for determination of hCG.

The reaction of the antibody and antigen depends on the incubation temperature and incubation time. Considering the convenience of the immunoassays for the future application, room temperature was selected throughout the experiment. As shown in Fig. 6(c), the results demonstrated that with increasing incubation time, the amperometric signal increased at the first 80 min, and tended to level off due to the saturated formation of antigen-antibody complex. Therefore, the incubation time of 2 h was chosen for the determination of hCG.

(Fig. 6)

Sensitivity of the immunosensor

Under optimal conditions, the current change increased with the increment of hCG concentration. As expected, the amperometric signal increased linearly with hCG concentration over the range of 0.05-50 ng mL^{-1} with a detection limit of 3.2 pg mL^{-1} at a signal-to-noise ratio of 3 (Fig. 7). Therefore, the immunosensor exhibited higher sensitivity. Some possible explanations might be considered as followed: (1) the excellent film-forming ability, adsorption capabilities and biocompatibility of CS might help the detection of hCG; (2) $BMIMPF_6$ not only could be good solvent but also acted as a suitable charge-transfer bridge to facilitate the electrode transfer rate; (3) MWCNTs-$BMIMPF_6$ composites were used as effective load matrix for the deposition of NP-Pd; (4) NP-Pd with lots of porous could display a high surface-to-volume ratio and could enhance the immobilized quantity of Ab, which improved the amperometric signal greatly; (5) The good electron transfer ability of MWCNTs and NP-Pd resulted in the dual-amplification effects; Additionally, the proposed method for the determination of hCG was compared with the previously reported methods in Table 2. The proposed method had a relative high sensitivity and low detection limit, which was a promising sensitive method to quantify hCG.

(Fig. 7)

(Table 2)

Specificity, Reproducibility and Stability

Specificity is an important criterion for immunosensors. Other possible interferents such as CEA, AFP, BSA, urea, L-tyrosine sulfate, DL-typtophan and Vc, etc, were investigated. The immunosensors were separately exposed to 10 ng mL^{-1}

hCG solutions with and without 50 ng mL^{-1} interference. As shown in Fig. 8, no remarkable changes were observed. Result indicated that the specificity of the present immunoassay protocol was satisfactory.

(Fig. 8)

Reproducibility is a key factor for developing a practical immunosensor. The intra-assay precision was evaluated by analyzing three hCG levels for five replicate measurements. The relative standard deviations (RSDs) were 4.9%, 3.8% and 5.1% for 5.0, 10.0 and 20.0 ng mL^{-1} hCG. Similarly, the inter-assay precision was evaluated by analyzing the same hCG level with five immunosensors made using the same conditions independently. The RSDs were 3.8%, 4.5%, and 4.2% for 5.0, 10.0 and 20.0 ng mL^{-1} hCG. The results obtained were acceptable.

The stability of the immunosensor was also examined. When it was not in use, it was stored at 4 ℃. The response of the immunosensor was retained 85% of the initial response after 2 weeks. The immunosensor kept long-term stability, which might be on account of the biocompatibility of NP-Pd.

Application of hCG immunosensor in human serum samples

The feasibility of the immunoassay for clinical applications was investigated by standard addition methods in human serum. The analytical results were shown in Table 3. The recovery efficiency was in the range of 96%-104.55%. Therefore, the proposed immunosensor could be satisfactorily applied to the clinical determination of hCG in real sample.

(Table 3)

Conclusions

In this work, a simple and sensitive electrochemical immunosensor using MWCNTs-BMIMPF$_6$/NP-Pd as a sensor platform to sequentially immobilize antibody was developed for hCG detection. The structure of MWCNTs-BMIMPF$_6$ and NP-Pd were characrized by EDS, XRD, SEM, TEM and BET analysis. The synergy of MWCNTs and IL could greatly enhance the conductivity. And MWCNTs-BMIMPF$_6$ composites acted as effective load matrix for NP-Pd. Moreover, NP-Pd with good biocompatibility could display a high surface-to-volume ratio, which could enhance the immobilized quantity of Ab. The proposed immunosensor showed high sensitivity, wide linear range, good reproducibility, acceptable precision and accuracy. The presented strategy was demonstrated to be simple and specific, which provided a novel promising platform of clinical immunoassay for hCG.

Acknowledgement

This project was financially supported by Shandong Provincial Natural Science Foundation, China (Grant No. ZR2012BL11), Shandong Provincial Science and Technology Development Plan Project, China (Grant No. 2013GGX10705) and the National Natural Science Foundation of China (Grant Nos. 51003040 and 51102114).

References

1 G. G. Yang, X. Y. Yang, C. Y.Yang, Y. H. Yang, *Colloids Surf. A*, 2011, **389**, 195-200.

2 X. K. Ding, K. L. Yang, *Anal. Chem.*, 2013, **85**, 10710-10716.

3 J. F. Wang, R. Yuan, Y. Q. Chai, S. R. Cao, S. Guan, P. Fu, L. G. Min, *Biochem. Eng. J.*, 2010, 51, 95-101.

4 Y. H. He, Y. P. Li, X. Hun, *Microchim. Acta*, 2010, **171**, 393-395.

5 J. Y. Hou, T. C. Liu, Z. Q. Ren, M. J. Chen, G. F. Lin, Y. S. Wu, *Analyst*, 2013, **138**, 3697-3704.

6 A. H. Liang, M. J. Zou, Z. L. Jiang, *Talanta*, 2008, **75**, 1214-1220.

7 S. C. Zhang, C. Z. Zhang, Z. Xing, X. R. Zhang, *Clin. Chem.*, 2004, **50**, 1214-1221.

8 M. L. Tao, X. F. Li, Z. S. Wu, M. Wang, M. Hua, Y. H. Yang, *Clin. Chim. Acta*, 2011, **412**, 550-555.

9 T. A. Wani, I. A. Darwish, *New J.Chem.*, 2012, **36**, 1114-1120.

10 S. Teixeira, G. Burwell, A. Castaing, D. Gonzalezb, R. S. Conlan, O. J. Guy, *Sens. Actuators B*, 2014, **190**, 723-729.

11 K. Sunil, Arya, M. K. Park, *Biosens. Bioelectron.*, 2014, **61**, 260-265.

12 S. F. Liu, Y. Lin, T. Liu, C. B. Cheng, W. J. Wei, L. Wang, F. Li, *Biosens. Bioelectron.*, 2014, **56**, 12-18.

13 R. Genc, D. Murphy, A. Fragoso, M. Ortiz, C. K. O'Sullivan, *Anal. Chem.*, 2011, **83**, 563-570.

14 U. Jarocka, R. Sawicka, A. Góra-Sochacka, A. Sirko, et al., *Biosens. Bioelectron.*, 2014, **55**, 301-306.

15 T. N. Lien, Truong, M. Chikae, Y. Ukitaa, Y. Takamura, *Talanta*, 2011, **85**, 2576-2580.

16 X. Y. Zhang, G. Y. Shen, S. Y. Sun, Y. M. Shen, C. X. Zhang, A. G. Xiao, *Sens. Actuators B*, 2014, **200**, 304-309.

17 R. Li, D. Wu, H. Li, C. X. Xu, et al., *Anal. Biochem.*, 2011, **414**, 196-201.

18 T. T. Qi, J. F. Liao, Y. S. Li, J. R. Peng, et al, Biosens. *Bioelectron.*, 2014, **61**, 245-250.

19 R. Feng, Y. Zhang, H. Q. Yu, D. Wu, H. M. Ma, et al., *Biosens. Bioelectron.*, 2013, **42**, 367-372.

20 E. Turkmen, S. Z. Bas, H. Gulceb, S. Yildiz, *Electrochim. Acta*, 2014, **123**, 93-102.

21 K. K. Liu, J. R. Zhang, Q. Liu, H. P. Huang, *Electrochim. Acta*, 2013,**114**, 448-454.

22 M. Li, M. Zhang, S. G. Ge, M. Yan, J. H. Yu, J. D. Huang, S. Liu, *Sens. Actuators B*, 2013, **181**, 50-56.

23 C. X. Xu, Q. Li, Y. Q. Liu, J. P. Wang, H. R. Geng, *Langmuir*, 2012, **28**, 1886-1892.

24 C. X. Xu, Y. Q. Liu, J. P. Wang, H. R. Geng, *J. Power Sources*, 2012, **199**, 124-131.

25 F. L. Jia, C. F. Yu, L. Z. Zhang, *Electrochem. Commun.*, 2009, **11**, 1944-1946.

26 L. F. Liu, O. Albrecht, U. Gosele, *Electrochem. Commun.*, 2010, **12**, 835-838.

27 J. S.Yu, Y. Ding, M. W. Chen, *Chem. Mater.*, 2008, **20**, 4548-4550.

28 S. Zang, Y. J. Liu, M. H. Lin, J. L. Kang, Y. M. Sun, H. T. Lei, *Electrochim. Acta*, 2013, **90**, 246-253.

29 L. Hou, Y. L. Cui, M. D. Xu, Z. Q. Gao, J. X. Huang, D. P. Tang, *Biosens. Bioelectron.*, 2013, **47**, 148-156.

30 E. Mojdeh, A. Mohammad, Khalilzadeh, K. M. Hassan, *Food Chem.*, 2013, **141**, 4311-4317.

31 J. J. Lu, S. Q. Liu, S. G. Ge, M. Yan, J. H. Yu, X. T. Hu, *Biosens. Bioelectron.*, 2012, **33**, 29-35.

32 P. Yanez-Sedeno, Pingarron, J. Riu, F. Rius, *Anal. Chem.*, 2010, **29**, 939-953.

33 L. Zhou, J. P. Wang, L. Gaia, D. J. Li, Y. B. Li, *Sens. Actuators B*, 2013, **181**, 65-70.

34 E. Lahiff, C. Lynam, N. Gilmartin, R. O'Kennedy, D. Diamond, *Anal. Bioanal. Chem.*, 2010, **39**, 1575-1589.

35 F. Xiao, F. Q. Zhao, J. W. Li, L. Q. Liu, B. Z. Zeng, *Electrochim. Acta*, 2008, **53**, 7781-7788.

36 B. Haghighi, H. Hamidi, L. Gorton, *Electrochim. Acta*, 2010, **55**, 4750-4757.

37 X. L. Niu, W. Yang, H. Guo, J. Ren, J. Z. Gao, *Biosens. Bioelectron.*, 2013, **41**, 225-231.

38 X. H. Liu, Z. Ding, Y. H. He, Z. H. Xue, X. P. Zhao, X. Q. Lu, *Colloids Surf. B*, 2010, **79**, 27-32.

39 C. X. Xu, A. H. Liu, H. J. Qiu, Y. Q. Liu, *Electrochem. Commun.*, 2011, **13**, 766-769.

40 J. Y. Wang, H. B. Chu, Y. Li, *ACS Nano*, 2008, **2**, 2540-2546.

41 T. Fukushima, A. Kosaka, Y. J. Ishimura, T. Yamamoto, T. Takigawa, N. Ishii, T. Aida, *Science*, 2003, 2072-2074.

42 J. C. Ma, D. A. Dougherty, *Chem. Rev.*, 1997, **97**, 1303-1324.

43 T. Fukushima, T. Aida, *Chem. OEur. J.*, 2007, **13**, 5048-5058.

44 S. Bellayer, J.W. Gilman, N. Eidelman, S. Bourbigot, X. Flambard, et al., *Adv. Funct. Mat.*, 2005, **15**, 910-916.

45 C. X. Xu, J. P. Wang, J. H. Zhou, *Sens. Actuators B*, 2013, **182**, 408-415.

46 X. Y. Li, Y. X. Liu, L. C. Zheng, M. J. Dong, Z. H. Xue, X. Q. Lu, X. H. Liu, *Electrochim. Acta*, 2013, **113**, 170-175.

47 S. MansouriMajda, H. Teymourian, A. Salimi, R. Hallaj, *Electrochim. Acta*, 2013, **108**, 707-716.

48 M. Elyasi, M. A. Khalilzadeh, H. Karimi-Maleh, *Food Chem.*, 2013, **141**, 4311-4317.

Figure captions

Scheme 1. Illustration of the stepwise immunosensor fabrication process.

Fig. 1. SEM images of (a) MWCNTs and (b) MWCNTs-$BMIMPF_6$ dispersed in CS and DMF by sonication.

Fig. 2. Structure of $BMIMPF_6$

Fig. 3. EDS spectra (a), XRD patterns (b), SEM (c), TEM (d) (e) and pore size distribution (f) of NP-Pd.

Fig. 4. CVs of (a) bare GCE; (b) MWCNTs/GCE; (c) MWCNTs-$BMIMPF_6$/GCE; (d) NP-Pd/GCE; (e) NP-Pd/ MWCNTs/GCE; (f) NP-Pd/MWCNTs-$BMIMPF_6$/GCE.

Fig. 5. A: CVs of (a) bare GCE; (b) Ag/BSA/Ab/NP-Pd/MWCNTs-$BMIMPF_6$/GCE; (c) MWCNTs-$BMIMPF_6$/GCE; (d) BSA/Ab/NP-Pd/MWCNTs-$BMIMPF_6$/GCE; (e) Ab/NP-Pd/MWCNTs-$BMIMPF_6$/GCE; (f) NP-Pd/MWCNTs-$BMIMPF_6$/GCE;

B: EIS of (a) NP-Pd/MWCNTs-$BMIMPF_6$/GCE; (b) Ab/NP-Pd/MWCNTs-$BMIMPF_6$/GCE; (c) BSA/Ab/NP-Pd/MWCNTs-$BMIMPF_6$/GCE; (d) MWCNTs-$BMIMPF_6$/GCE; (e) Ag/BSA/Ab/NP-Pd/MWCNTs-$BMIMPF_6$/GCE; (f) bare GCE. Conditions: PBS (pH 7.2) containing 0.2 M KCl and 5 mM $K_3[Fe(CN)_6]$.

Fig. 6. Effect of (a) the mass ratio of MWCNTs and $BMIMPF_6$, (b) the pH value, (c) the incubation time of antibody and antigen on the electrochemical signal of the immunosensor.

Fig. 7. Calibration curve for hCG determination (n=3).

Fig. 8. Amperometric response of the immnosensor to interferents.

Figures and Schemes

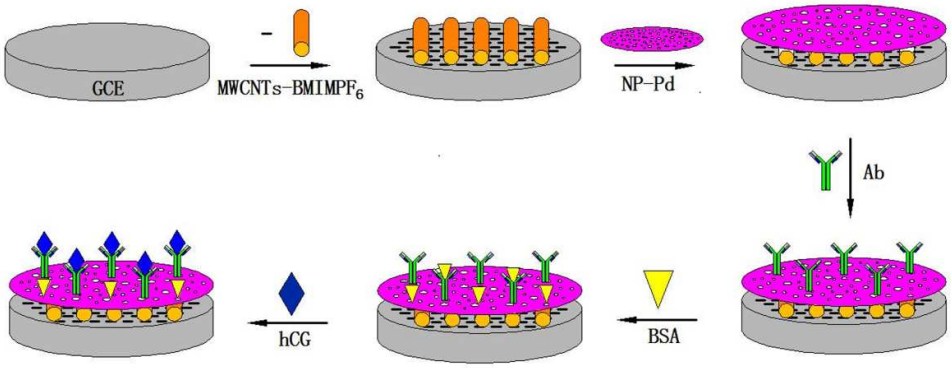

Scheme 1

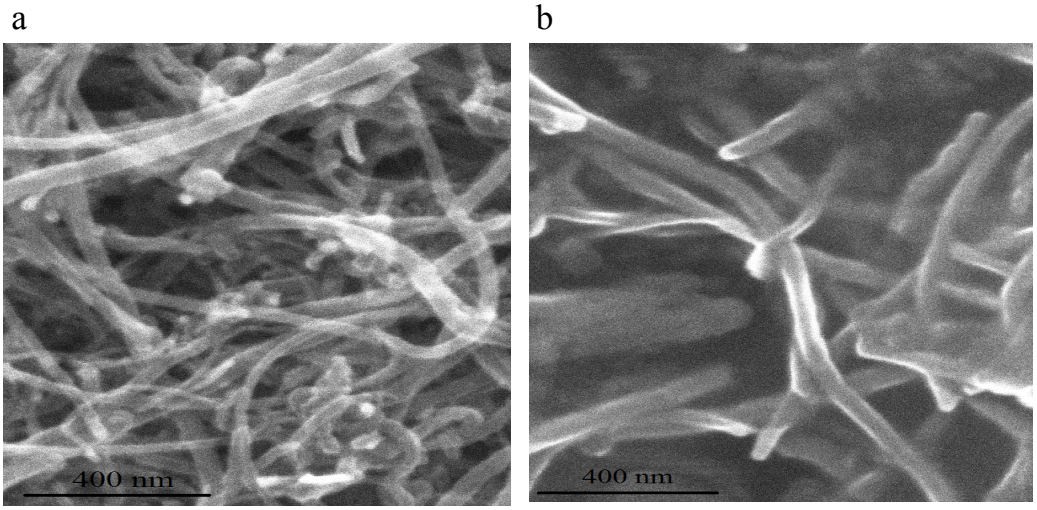

Fig. 1

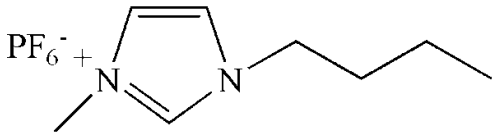

Fig. 2

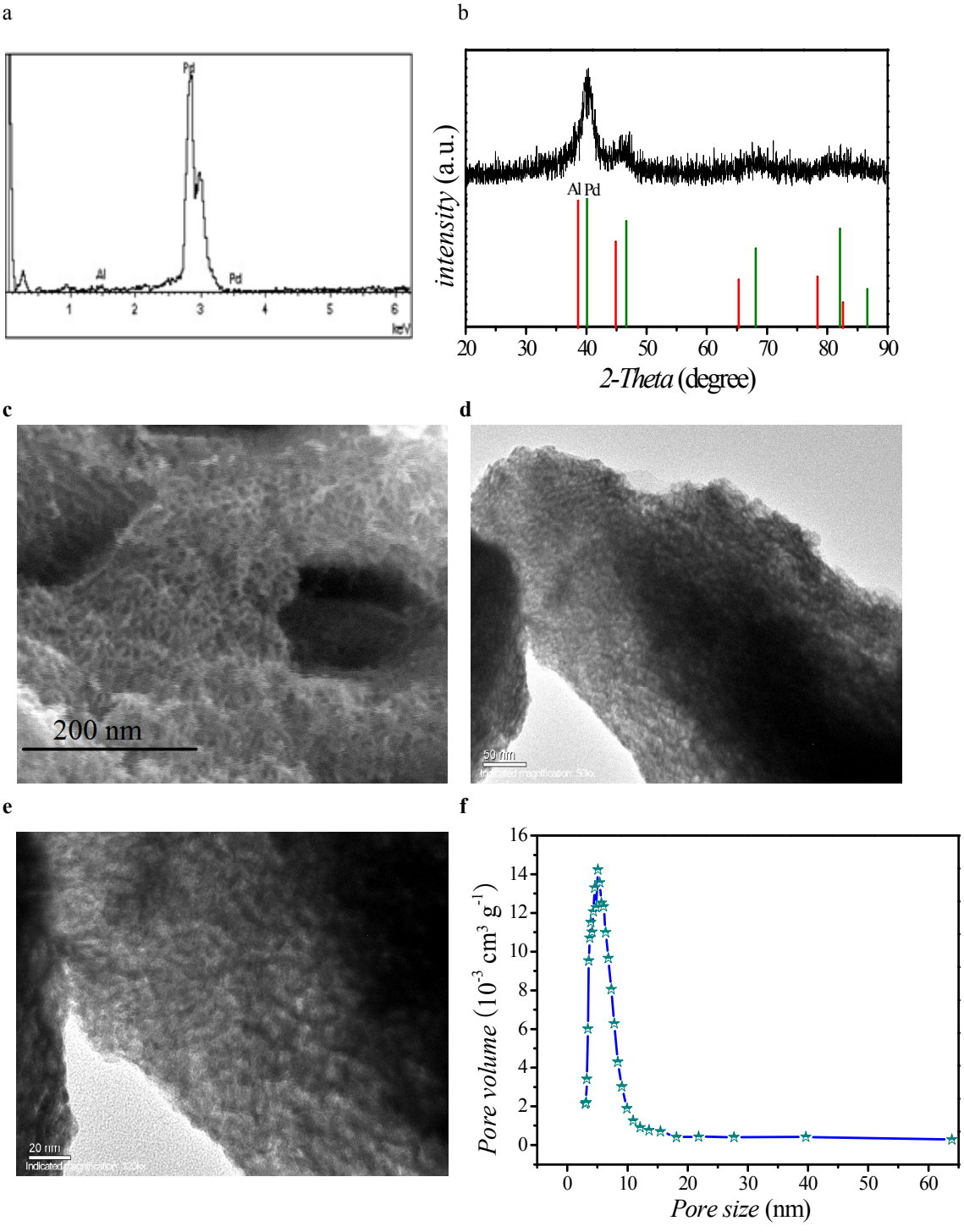

Fig. 3

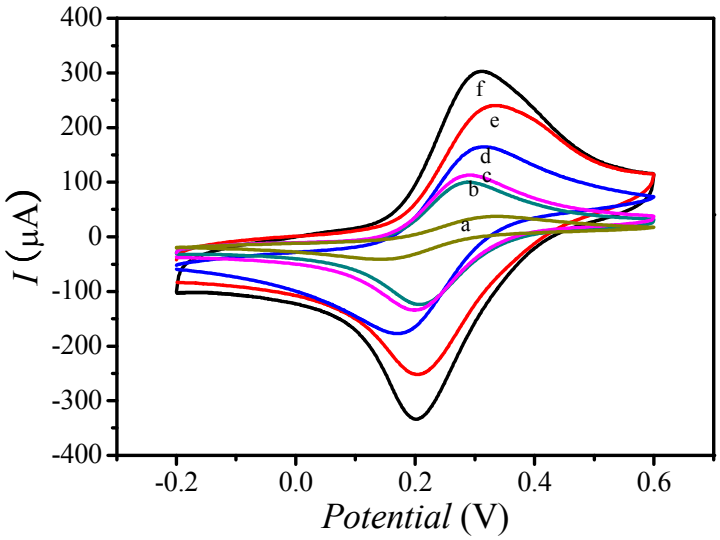

Fig. 4

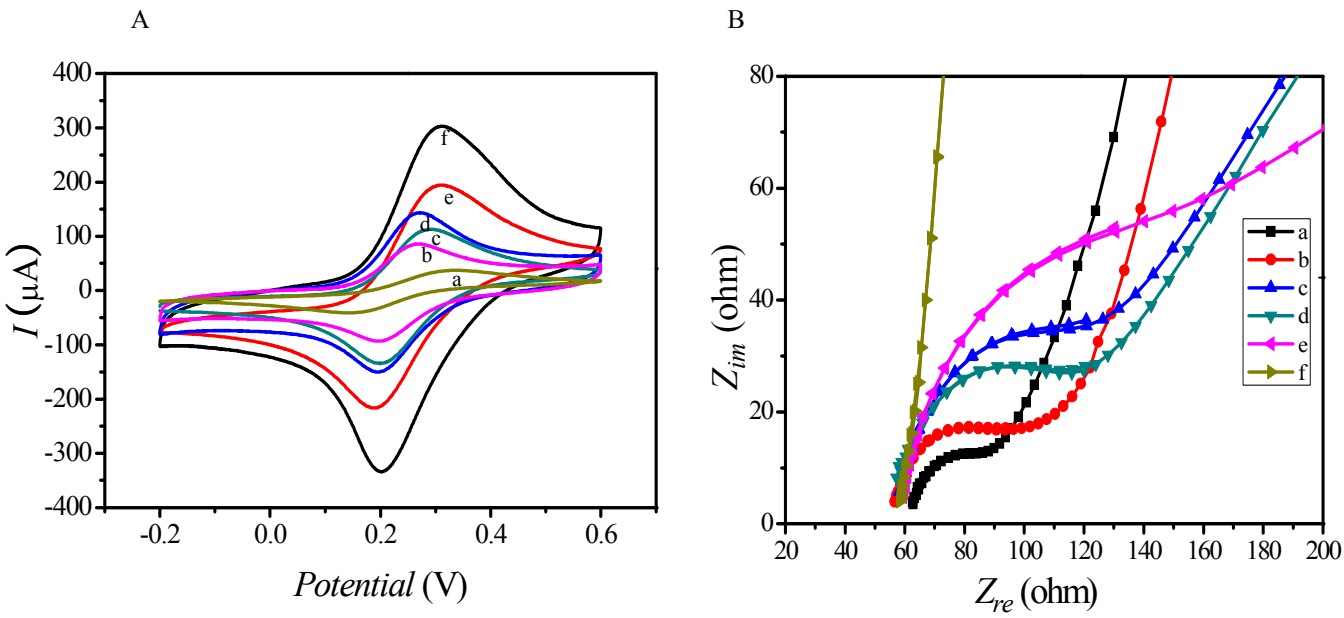

Fig. 5

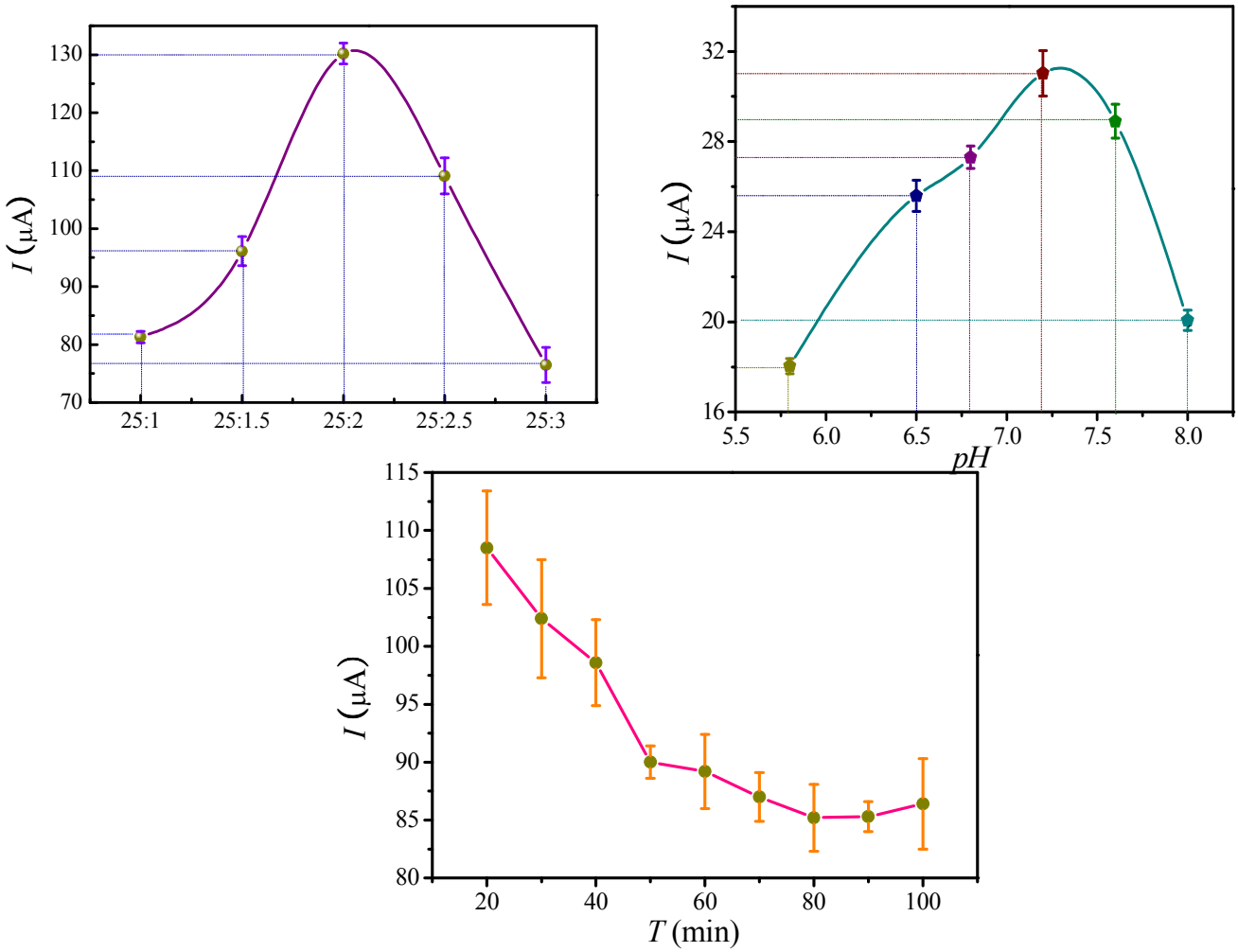

Fig. 6

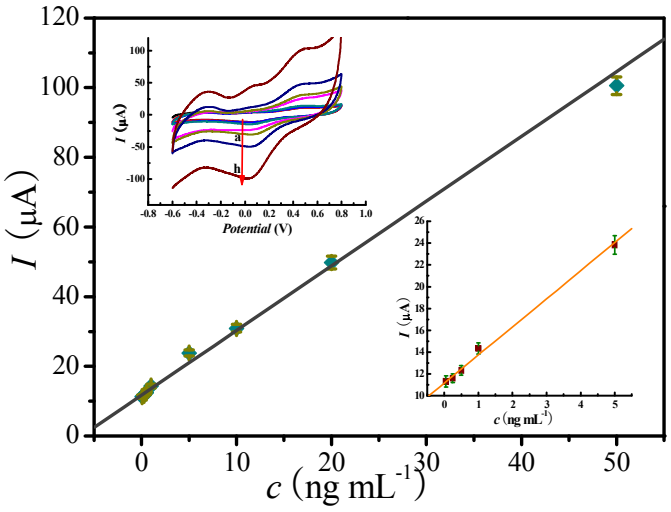

Fig. 7

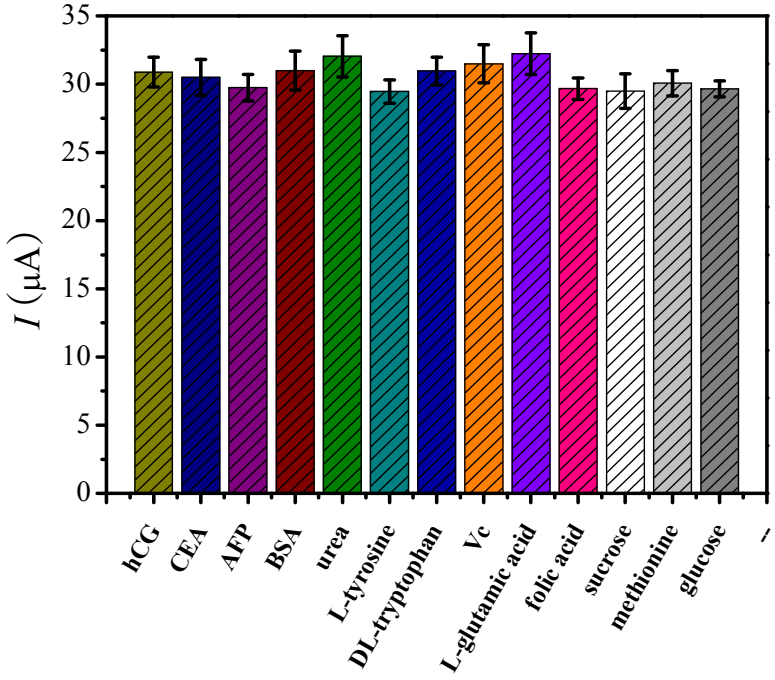

Fig. 8

Tables

Table 1 The surface coverage (Γ *) of different modified electrodes.

Electrode	A (cm^2)	Γ * (mol cm^{-2})
GCE	0.0663	2.546×10^{-8}
MWCNTs/GCE	0.177	2.859×10^{-8}
MWCNTs-$BMIMPF_6$/GCE	0.201	2.894×10^{-8}
NP-Pd /GCE	0.293	2.715×10^{-8}
NP-Pd/MWCNTs/GCE	0.426	3.348×10^{-8}
NP-Pd/MWCNTs-$BMIMPF_6$/GCE	0.538	3.504×10^{-8}

Table 2 Comparison of hCG determinations using the proposed and reference methods

Methods	Reagents or condition	Linear range	Detection limit	Reference
Fluoroimmunoassay	Magnetic particles	0.16-450 ng mL^{-1}	0.08 ng mL^{-1}	[5]
Resonance scattering spectral assay	Gold nanoparticles	2.5-208.3 mIU mL^{-1}	0.83 mIU mL^{-1}	[6]
Spectrometry	an inductively coupled plasma mass spectrometry	5.0–170 ug L^{-1}	1.7 ug L^{-1}	[7]
label-free electrochemical immunosensor	Pt–Au alloy nanotube	25-400 mIU mL^{-1}	12 mIU mL^{-1}	[8]
automated flow immunosensor	flow kinetic-exclusion analytical technology	0.2-50 ng mL^{-1}	0.2 ng mL^{-1}	[9]
immunosensor	epitaxial graphene	0.62-5.62 ng mL^{-1}	0.62 ng mL^{-1}	[10]
label-free electrochemical immunosensor	MWCNTs-$BMIMPF_6$ NP-Pd	0.05-50 ng mL^{-1} (0.5-500 mIU mL^{-1})	3.2 pg mL^{-1} (0.32 mIU mL^{-1})	Present work

Table 3 hCG determination in serum by the proposed immunosensor (n=5).

Amount added (ng mL^{-1})	This method (ng mL^{-1} ± RSD%)	Recovery (%)
0.5	0.48 ± 2.47	96
1.0	1.05 ± 3.89	105
5.0	5.23 ± 4.13	104.6
10.0	9.87 ± 3.43	98.7
20.0	20.91 ± 2.18	104.55